Hindawi
Journal of Nanomaterials
Volume 2019, Article ID 7328478, 9 pages
https://doi.org/10.1155/2019/7328478

Research Article

Gelatinous Siphon Sheath Templates the Starfruit-Shaped Aragonite Aggregate Growth

Zeng-Qiong Huang,[1] **Gang-Sheng Zhang**,[2] **and Yuan Tan**[2]

[1]*College of Pharmacy, Guangxi Medical University, Nanning, Guangxi 530021, China*
[2]*College of Materials Science and Engineering, Guangxi University, Nanning, Guangxi 530004, China*

Correspondence should be addressed to Zeng-Qiong Huang; huangzengqiong@163.com

Received 10 August 2018; Accepted 5 November 2018; Published 10 February 2019

Academic Editor: Jean M. Greneche

Biomimetic synthesis of aragonite with various templates *in vitro* is an important way to understand the biomineralization process and synthesize nacre-like materials. Herein, we used the siphon sheath from the bivalve *Lutraria sieboldii* as the substrate for the formation of calcium carbonate. We found that the inner layer of the sheath, which is composed of approximately 40% protein and 60% β-chitin, induced the formation of nearly pure aragonite by the transformation of amorphous calcium carbonate (ACC). More surprisingly, unique starfruit-shaped aragonite aggregates were observed on the substrate and were constructed from many adhered, oriented aragonite tablets. We consider that the acid-rich protein from the inner layer of the siphon sheath triggers the formation of ACC, and the swollen β-chitin regulates the transformation of ACC into aragonite by lattice matching and stereochemical recognition. The various surface adhesion energies of the crystal, the change in growth rates on different crystallographic facets, and the hexagonal features of the aragonite tablets led to the formation of starfruit-shaped aragonite aggregates.

1. Introduction

Biogenic calcium carbonate ($CaCO_3$) has attracted considerable scientific interest because of its outstanding mechanical properties and widespread distribution in nature. There are three common crystalline polymorphs of $CaCO_3$: the most stable form, calcite; the metastable form, aragonite; and the least stable form, vaterite. In addition, a hydrated amorphous calcium carbonate (ACC) was observed in sea urchins and nacre [1–5] and has also been artificially synthesized [6]. Nacre has been studied extensively in the past several decades [7–14] because of its renowned hierarchical, organic-inorganic composite structure, as well as its superior mechanical properties.

Inspired by the sandwich-like structure of nacre [7, 8], considerable effort has been devoted to *in vitro* biomimetic mineralization experiments in an effort to fabricate composite materials that are similar to nacre or to reveal the mechanism of biomineralization. The most common approach for these experiments is to use various substrates, such as chitin [15–17], collagen, silk fibroin [18–20], fibrous protein, gelatin [21–24], and nacre [25–27], to modulate the formation of $CaCO_3$ polymorphs. Furthermore, nacre protein with or without chitin has been used to induce $CaCO_3$ growth for an improved understanding of the interactions between crystals and proteins [6, 28–31]. However, to the best of our knowledge, the siphon sheath of the bivalve *Lutraria sieboldii* has never been used as a substrate for these *in vitro* biomimetic mineralization experiments.

The bivalve *L. sieboldii* has a noticeably long siphon that is longer than the shell itself. The siphon is protected by a sheath that is connected to the periostracum at the growth edges of the shell. Structurally, the semitransparent siphon sheath is divided into two layers: a thin, slightly sclerotized outer layer, which is similar to the periostracum, and a transparent, colorless inner layer with a swollen, gelatinous texture. This sheath is likely acting as the template for the nucleation and growth of the $CaCO_3$ for the shell.

In this study, we conducted *in vitro* experiments using the siphon sheath as a substrate in order to explore the

sheath's ability to modulate the formation of $CaCO_3$ polymorphs and their morphology. Interestingly, on the inner surface of the sheath, we observed starfruit-shaped aragonite aggregates (SFAA), which were constructed from the aggregation of oriented, attached aragonite tablets that had transformed from ACC. We consider that the acid-rich proteins and β-chitin from the gelatinous siphon sheath inner layer (SSIL) both induce the formation of ACC and regulate the transformation of ACC into aragonite. The transformation from ACC to aragonite is likely a universal phenomenon that exists not only in *in vitro* experiments [6, 21] but also in natural nacre growth [3–5].

2. Experimental

2.1. Sample Preparation. Fresh *L. sieboldii* samples were obtained from the seafood market of Nanning in Guangxi Province, southern China. The siphon sheaths were isolated from their shells, rinsed fully with deionized water, and used as the substrates in the biomimetic synthesis experiments. Prior to chemical composition analysis, the SSILs were separated from their outer layer, washed with deionized water, and freeze dried.

2.2. Amino Acid Composition Analysis. The dried SSILs were hydrolyzed in the presence of 6 M HCl at 110°C for 22 h. Next, the acid was removed and the hydrolysate was vacuum dried. The hydrolysate was redissolved in a sodium citrate buffer solution and analyzed with an amino acid analyzer (L-8800, Hitachi) [32].

2.3. Biomimetic Synthesis of $CaCO_3$. With their inner surfaces facing upward, the siphon sheaths were placed on the bottom of a culture dish containing 80 mL of calcium chloride solution (10 mM) [22]. For comparison, another culture dish was set up with only coverslips. Both of the culture dishes and a watch glass containing 10 g of ammonium carbonate were placed in a closed desiccator. $CaCO_3$ crystals were grown in ambient conditions via the diffusion of CO_2 into the calcium chloride solution for 24 h [33]. The substrates were collected, rinsed by deionized water, and air dried.

2.4. Characterization. The dried SSILs and the synthetic crystals were analyzed by FTIR (Nexus 470, Nicolet) with a resolution of 4 cm^{-1} over a scanning range of 500 to 2000 cm^{-1}. Crystal morphology was observed by an FESEM (SU8020, Hitachi) operating at 10 kV. After the substrates were treated with ultrasonication in absolute alcohol for 2 min, an HRTEM (JEM-2100F, JEOL) operating at 200 kV was used to determine the polymorph.

3. Results and Discussion

3.1. Amino Acid Composition Analysis. After freeze-drying, the gelatinous SSILs lost 97.67% of their weight, which implies that the gel has a good capacity for water absorption. Amino acid analysis of the gel presented an unexpectedly low amino acid content at only 37.58%, indicating that protein is not the primary component of the SSIL. Notably, however, the dicarboxylic amino acids, aspartic acid (Asp) and glutamic acid (Glu), had the highest content and accounted for 12.43% and 11.87% of the total, respectively (Table 1). This result is similar to a previous report, which showed a high content of Asp and Glu from the proteins within the SSIL of *Lutraria lutraria* (a close relative of *L. sieboldii*) [34]. These acidic amino acids might be involved in the formation of aragonite, as the fibrous protein of the bivalve ligament is also rich in Asp and Glu and can induce the formation of almost pure aragonite [21, 32].

Asp, Glu, and other hydrophilic amino acids accounted for 56.55% of the total, which is strikingly similar to the analysis of proteins from the SSIL of *L. lutraria* (57.60%) [34]. This hydrophilicity may contribute to the good water absorption capacity of the gelatinous inner layer. However, the ability for the proteins to absorb water is limited, since the overall protein content is less than 40%. The components within the remaining 62.42% of the total weight of the inner layer should play a more important role in the water absorption capacity and swellability.

Notably, the combined Ser, Gly, and Ala content is less than 50% of the total, indicating that the SSIL protein is not a silk-like protein [35] and is also different from nacre protein [8]. It is still not clear if there is a mixture of proteins or a single protein, and further studies are needed to reveal the nature of this unique protein.

3.2. FTIR Determination of the SSIL and Synthetic Crystals. An FTIR spectrum of the SSIL is shown in Figure 1(a). The spectrum shows three peaks at 1658, 1549, and 1317 cm^{-1}, which correspond to the amide I–III bands of the CONH group, respectively. The 4 bands at 1155, 1113, 1073, and 1032 cm^{-1} are assigned to the stretching modes of the C-O-C and C-O [36]. In addition, the peaks at 1378 and 617 cm^{-1} correspond to the rocking of the methyl group and an out-of-plane hydroxyl group, respectively [37, 38]. These peaks are consistent with the infrared absorption of chitin [36–38], which indicates that in addition to protein, chitin is a major component of the SSIL.

In nature, chitin primarily occurs as either the α- or β-allomorph. Generally, β-chitin is found associated to proteins in mollusks [7, 34, 39] and has a higher swelling and affinity towards solvents compared to α-chitin [40]. In our experiment, we observed that the chitin from the SSIL appears alongside the protein (or proteins) and possesses good water absorption abilities and swellability. These findings are consistent with a previous study, which showed that the SSIL of *L. lutraria* is a chitin-protein complex with a β-chitin content of 45% [34]. Therefore, we believed that the chitin from the SSIL of *L. sieboldii* also presents as the β-form. Since the SSIL is a chitin-protein complex, it may regulate the polymorph of $CaCO_3$ by a similar method to nacre, which also contains chitin and protein that could affect the morphology and polymorph of $CaCO_3$ [8].

The spectra of the synthetic crystals are shown in Figures 1(b) and 1(c). Obviously, the spectra of the crystals grown on coverslips show only characteristic calcite peaks at 713, 876, and 1432 cm^{-1} (Figure 1(b)), whereas the spectra of the crystals grown on the SSILs show only characteristic

Table 1: Amino acid compositions of the siphon sheath inner layer from *L. sieboldii* and *L. lutraria*.

Amino acid	*L. sieboldii* (g/100 g)	*L. lutraria* (residues/1000 residues) [34]
Asp	4.67	133
Thr	2.4	112
Ser	1.88	143
Glu	4.46	100
Pro	2.29	47
Gly	1.82	90
Ala	1.46	60
Cys	1.76	—
Val	2.39	46
Met	3.04	Trace
Ile	1.54	63
Leu	1.95	84
Tyr	2.24	3
Phe	1.84	31
Lys	2.07	54
His	0.46	0
Arg	1.31	27
Total	37.58	993

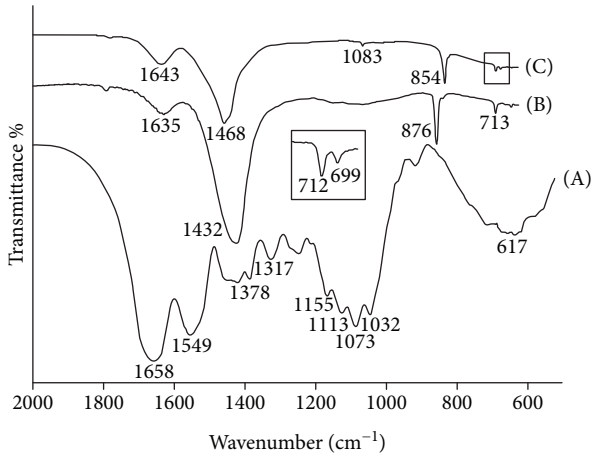

Figure 1: FTIR spectra of (a) the siphon sheath inner layers, (b) crystals grown on coverslips, and (c) crystals grown on siphon sheaths. (a) Peaks corresponding to chitin and protein are shown in (a). Characteristic peaks of calcite and aragonite are shown in (b) and (c), respectively.

aragonite peaks at 699, 712, 854, 1083, and 1468 cm^{-1}, indicating the formation of pure aragonite (Figure 1(c)). Coincidentally, we obtained similar results when we used the fibrous protein from a bivalve ligament as the substrate [21]. Although the fibrous protein and SSIL are from different bivalve species, both of them are water insoluble, rich in acidic amino acids, and occur in the crystallographic β-form [32, 34]. These common characteristics are likely the key factors controlling the formation of pure aragonite [28].

3.3. SEM Observation of Synthetic Crystals. Although a sampling time of 24 h was used in all biomimetic experiments, the aragonite crystals that were grown on the siphon sheath had various morphologies, which were observed by SEM (Figures 2(a)–2(c)). This variety is caused by the different nucleation times and growth stages of the distinct crystals. During the early growth stage, the aragonite crystals are constructed of many lamellas and have an irregular shape with a length and width of 1.65 and 0.89 μm, respectively (Figures 2(a) and 3(a)). Interestingly, as the crystals grew, an unusual starfruit-shaped aragonite with a length and width of up to 3.38 μm and 1.58 μm, respectively, was found on the SSIL substrate (Figures 2(b) and 2(c)). This unique structure was made of many lamellar aragonite crystals (Figures 3(b) and 3(c)). In addition, the concavity between two ridges of an immature starfruit-shaped aragonite was covered by several amorphous substances (Figure 3(b)). These amorphous substances are likely ACC, since there were no other additives in the reaction solution and the SSIL substrate is water insoluble. Therefore, we deduced that the lamellar aragonite crystals were formed by the transformation of ACC, and the subsequent aggregation of aragonite crystals produces the SFAA.

With increased crystallization time, SFAA gradually developed into spindle-shaped structures, with lengths ranging from 4.19 μm to 6.60 μm and widths ranging from 1.88 μm to 2.61 μm, respectively (Figures 2(b) and 2(c)). These spindle-shaped structures are strikingly similar to those grown on the inner surface of the shell periostracum from natural *L. sieboldii* (Figure 4). This similarity demonstrates the template-induced growth of aragonite in the bivalve shell, and the siphon sheath may act as the substrate that induces the nucleation and growth of $CaCO_3$ for the shell. Based on our observations, we concluded that the SFAA is a transition state in the formation of the spindle-shaped aragonite aggregates.

The SEM image of crystals grown on coverslips (Figure 2(d)) shows only perfect rhombohedral calcite, which supports our previous analysis [21].

3.4. Observation on the Tip of SFAA. Figure 5 shows the fine structure of the tip of the SFAA. Clearly, a relatively mature SFAA with six ridges was built from many aragonite nanoparticles (Figure 5(a)). These nanoparticles adhered in a ladder-like orientation that extends from the tip of the aggregate to the middle (Figure 5(b)). Some of these nanoparticles retained the hexagonal structure of the aragonite tablets, and the tablets distant from the tip were wider than those near the tip (Figure 5(b)). Even more remarkably, ACC was also observed attached to the tip and the side edge of adjacent aragonite aggregates (Figure 5(a)), which suggests that the aragonite crystal was transformed from ACC. These observations suggest that SFAA grows three dimensionally.

Similar to the relatively mature SFAA, the vertical view of an immature SFAA shows a perfect hexagonal structure constructed from a large number of stacked aragonite tablets (Figures 5(c) and 5(d)). These adhered aragonite tablets are oriented to hexagonal or pseudohexagonal structures,

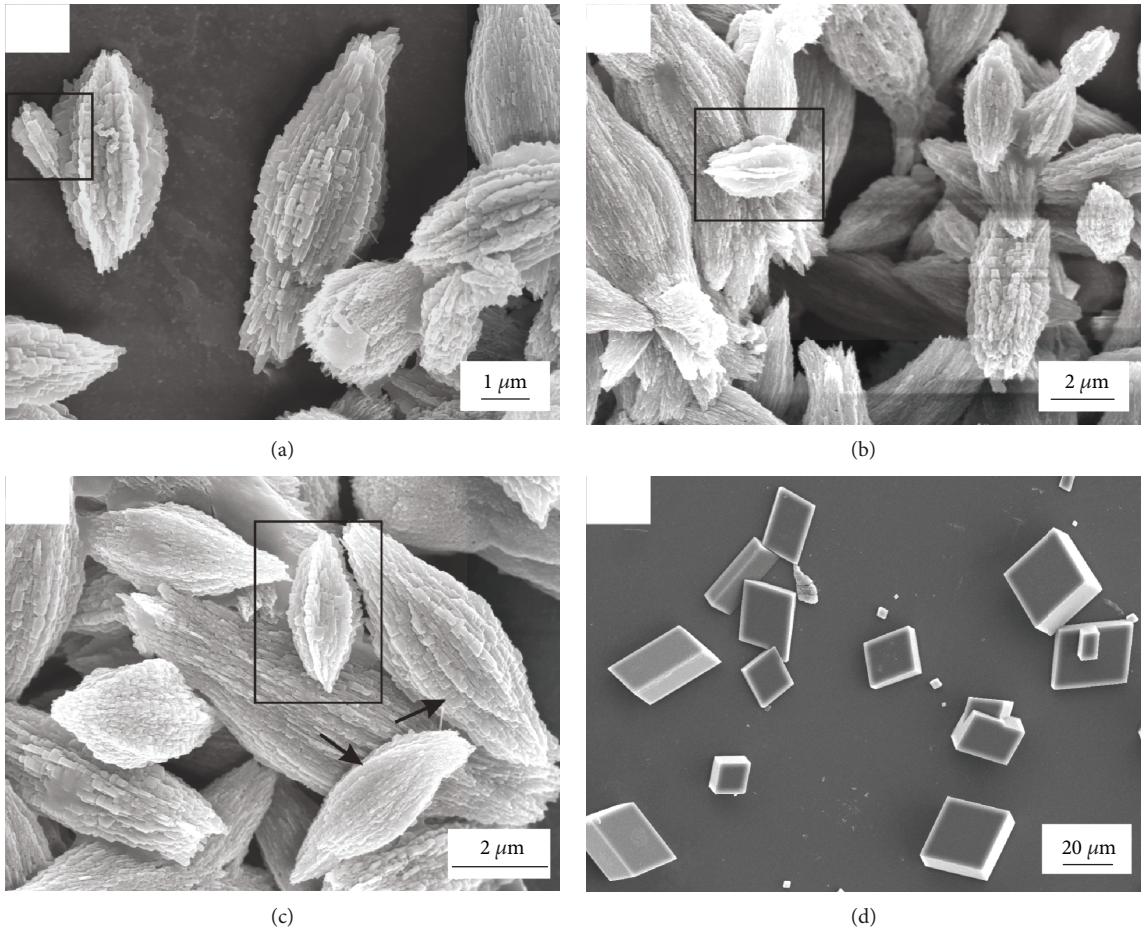

(a) (b) (c) (d)

Figure 2: SEM images of crystals grown on a siphon sheath (a-c) and on a coverslip (d) for 24 h. Aragonite crystals that developed from an irregular shape to starfruit-shaped and spindle-shaped structures (as indicated by black arrows) are shown from (a) to (c). A rhombohedral calcite is shown in (d).

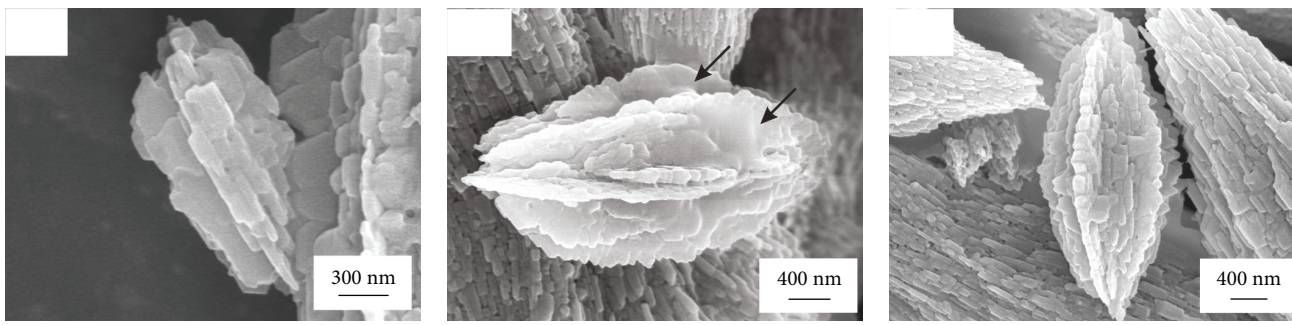

(a) (b) (c)

Figure 3: Enlarged views of the boxed areas in Figures 2(a)-2(c). An aragonite with an irregular shape is shown in (a). (b) An immature starfruit-shaped aragonite aggregate made up of lamella and covered by ACC (black arrows) is shown in (b). A mature starfruit-shaped aragonite aggregate built from many lamellas is shown in (c).

similar to those in nacre, and the tablets distant from the tip are thicker and bigger than those near the tip (Figure 5(d)). In addition, tablets at the tip exhibit an irregular shape, which indicates that they are newly formed crystals. These observations demonstrated that aragonite tablets primarily stack parallel to the long axis of the SFAA, and the SFAA on the long axis grows from the middle to the two tips.

This is not the first time that a starfruit-shaped structure was found. For example, lead wolframate ($PbWO_4$) and gold nanorods and nanowires with a starfruit shape have been synthesized [41, 42]. Starfruit-like vanadium oxide (VO_2) with high-power capability and good cycling stability for supercapacitor applications has been reported [43]. Although we have not determined the properties of the

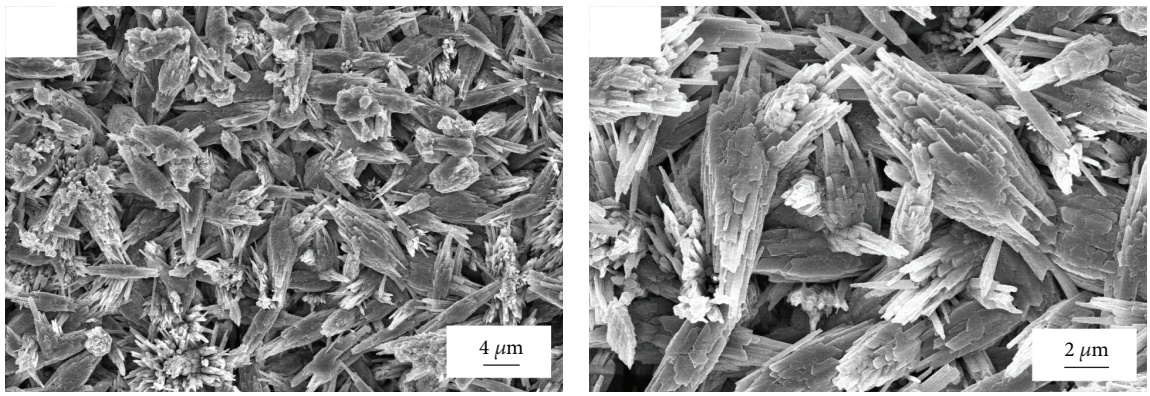

(a) (b)

Figure 4: SEM images of aragonite crystals grown on the inner surface of a *L. sieboldii* shell periostracum in nature. (a) Many of the spindle-shaped aragonite crystals are similar to those grown on the siphon sheath in Figure 2. (b) Enlarged view of (a) shows the detailed structure of the spindle-shaped aragonite.

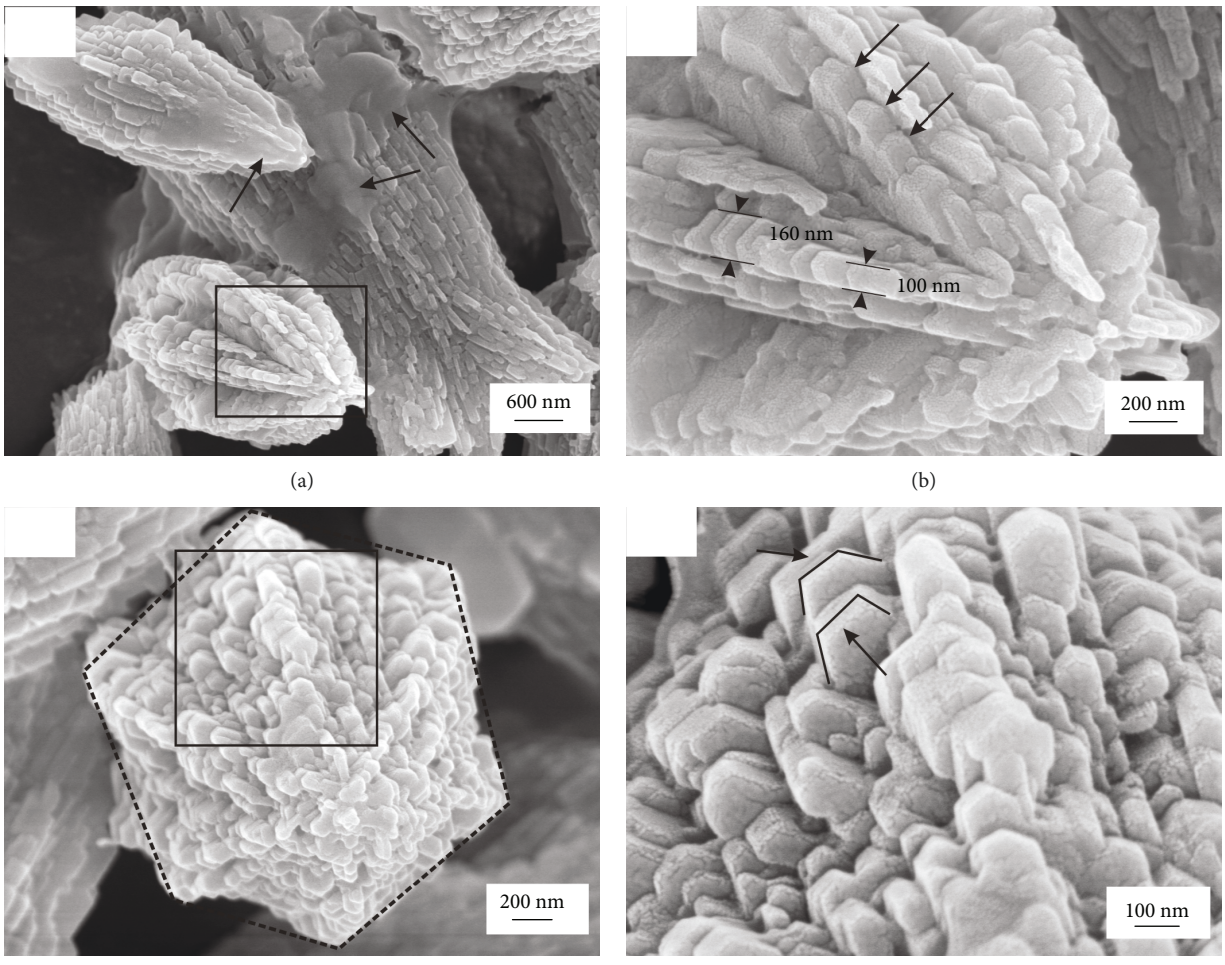

(a) (b)

(c) (d)

Figure 5: SEM images of the tip of the SFAA: (a) an SFAA and other aragonite aggregates covered by ACC (indicated by black arrows); (b) detailed view of the boxed area in (a) shows that the SFAA was formed by oriented, adhered nanoparticles (black arrows indicate the ladder-like adhesion); (c) vertical view of an immature SFAA shows its hexagonal structure; (d) enlarged view of the boxed area in (c) shows hexagonal aragonite tablets stacking one by one along the long axis of an SFAA.

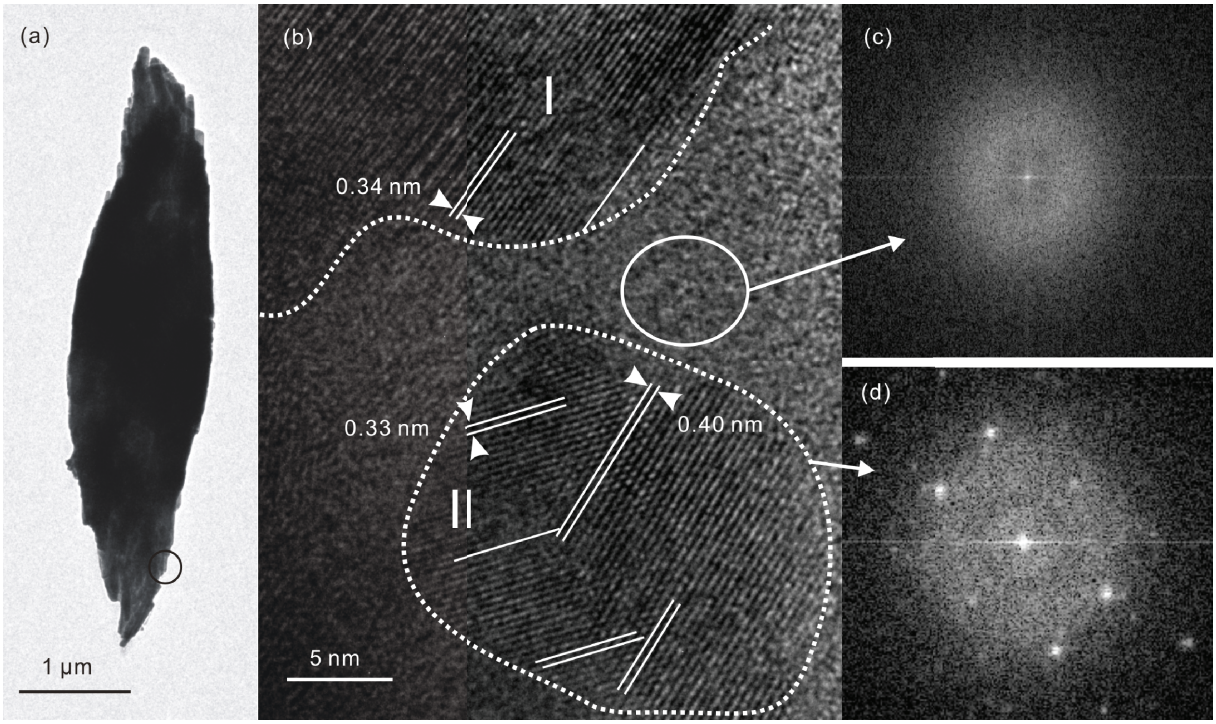

Figure 6: (a) TEM image of a spindle-shaped aragonite aggregate. (b) HRTEM image of the black circular area in (a), where the nanocrystals are numbered and outlined with dashed lines. In zone II, two sets of lattice fringes were shown, and lattice fringes extend across two adjacent nanocrystals. (c, d) Fast Fourier transform (FFT) patterns of related areas in (b). The former shows a diffuse halo, indicating that the internanocrystal space is filled with amorphous material, while the latter shows clear spots, representing a crystalline texture.

SFAA, this unique structural feature will endow the crystals with excellent mechanical performance or other properties. In a future study, we should focus on the synthesis of SFAA in the absence of templates.

3.5. TEM Observation on the Tip of the Aragonite Aggregate. To confirm our hypothesis that ACC transforms into an aragonite crystal, HRTEM was performed. Figure 6(a) displays a synthetic spindle-shaped aragonite aggregate with a dark middle and two slightly bright tips, which implies that the middle of the aggregate has better crystallinity and is therefore more mature than the tips. The HRTEM image of the tip (Figure 6(b)) shows that it is partially crystallized, with a small amount of amorphous material filling the internanocrystal space, as confirmed by the diffuse halo in the fast Fourier transform (FFT) pattern (Figure 6(c)). Because no organic additives were used in our experiment, this amorphous material is ACC.

Notably, the crystallized portion was divided into two zones (I and II), which each show clear lattice fringes with distinct interplanar spacing (Figure 6(b)). This finding indicates that nanocrystals in different zones are nucleated independently; therefore, nanocrystals in zones I and II are misoriented to each other, as shown by their respective lattice fringe orientations of 0.34 nm and 0.40 nm (Figure 6(b)). Interestingly, two sets of clear lattice fringes are shown in zone II, indicating the contact of two nanocrystals. In addition, these two adjacent nanocrystals share common lattice fringes (0.40 nm) at the place where they intersect, suggesting that they formed a large crystal by oriented attachment [44]. This finding was confirmed by the FFT pattern, which exhibits clear spot scattering, similar to a single crystal (Figure 6(d)). Our observations indicate that the aragonite crystal was transformed from ACC, and the nanocrystals that build the spindle-shaped aggregate or SFAA should be aggregated by oriented attachment.

The SFAA is rare, and to the best of our knowledge, it has never been reported in previous studies where aragonites were grown on other substrates. Although there are different morphologies in the synthetic aragonite aggregates, they are initially formed from the adhered oriented nanoparticles and then gradually change into different structures. It appears that this growth pattern is unrelated to the substrates that were used; therefore, how does the SSIL control the transformation of ACC into aragonite crystals and regulate the formation of the unusual SFAA?

3.6. Possible Mechanism of SFAA Formation. As mentioned above, both the SSIL and ligament fibrous protein contained acidic amino acids and possessed β-sheet structural units. Therefore, we believe that the regulative function of the SSIL on the $CaCO_3$ polymorph will be similar to that of the ligament fibrous protein [21]. In other words, the acidic amino acids of the protein (or proteins) from the SSIL attract and bind Ca^{2+}, triggering the formation of ACC on the surface of the SSIL (Figure 7(a)). Next, the water-insoluble β-chitin, the interchain spacings of which are 0.485 nm and 0.80 nm-0.86 nm (swollen) in the *ab* plane

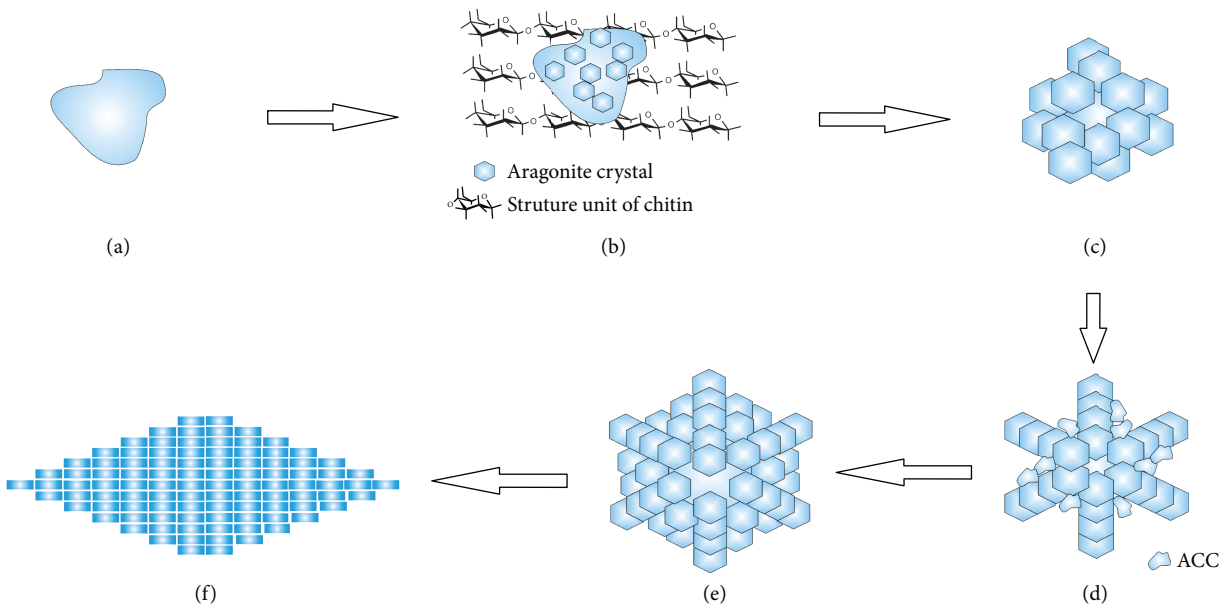

Figure 7: Schematic of the possible formation process of aragonite aggregates: (a) ACC formed on the surface of substrate; (b) ACC transformed into aragonite crystals by the β-chitin template; (c) aragonite crystals aggregate, orient, and attach to form an irregularly shaped structure (vertical view); (d, e) starfruit-shaped structure formed by adhered oriented crystals and continuous adhesion of ACC, as well as the transformation of ACC into aragonite crystals (vertical view); and (f) the starfruit-shaped structure develops gradually into a spindle-shaped structure (longitudinal view).

[45], provides a template that promotes the transformation of ACC into aragonite, which has a similar lattice ($a = 0.496$ nm and $b = 0.798$ nm), by lattice matching and stereochemical recognition (Figure 7(b)) [20, 21]. After that step, ACC continuously attaches to the surface of the aragonite crystals and assemble new crystals by oriented attachment and three-dimensional growth, ultimately forming nanorods and irregularly shaped aragonite aggregates (Figure 7(c)).

We suggest that the evolution of the morphology from an irregular shape to a starfruit shape is caused by the different surface adhesion energies of the crystals [46] and the variation in the growth rates on different crystallographic facets [47]. Although the typical morphology of an aragonite tablet is hexagonal, most of the aragonite crystals present as pseudohexagonal tricrystals. Consequently, these irregular structures evolve into starfruit-shaped structures with six ridges (Figure 7(d)). These ridges promote the deposition of both ACC and crystals on the concavities between two adjacent ridges because the surface energies at the concavities are higher than at the ridges, and crystals are inclined to nucleate on concavities with lower surface energies (Figures 7(d) and 7(e)). With increased crystallization time, increasing numbers of crystals formed on the concavities and attached the two tips of the SFAA, resulting in the formation of a spindle-shaped structure (Figure 7(f)).

4. Conclusions

Starfruit-shaped aragonite aggregates were synthesized without any additives, and a gelatinous siphon sheath from the bivalve *L. sieboldii* was used as the substrate. The siphon sheath is composed of an outer and inner layer, the latter of which is a chitin-protein complex comprised of approximately 40% proteins and 60% β-chitin. The hydrophilic proteins and hydrophobic chitin provide the siphon sheath with good water absorption and swellability and ultimately control the nucleation of aragonite crystals. Our proposed mechanism for regulation begins with the acidic amino acids of the proteins triggering the formation of ACC. β-Chitin regulates the transformation of ACC into aragonite by both lattice matching and stereochemical recognition. The various surface adhesion energies of the crystal combined with the difference in growth rates for different crystallographic facets and the hexagonal structural features of the aragonite tablets cause the formation of starfruit-shaped aragonite aggregates.

Our findings suggest that the siphon sheath of the bivalve *L. sieboldii* may act as a substrate for the growth of pure aragonite and play an important role in the formation of shells. In future studies, we should focus on the structure of and interaction between β-chitin and proteins. Identifying and determining the structure of proteins in the siphon sheath is also highly important to further understand their role in biomineralization.

Data Availability

No data were used to support this study.

Conflicts of Interest

The authors declare that there is no conflict of interests regarding the publication of the manuscript.

Acknowledgments

We thank Dr. Chuanbai Yu of Guilin University of Technology for his assistance in HRTEM determination. This work was supported by the National Natural Science Foundation of China (grant number NSFC 31760248).

References

[1] S. Raz, P. C. Hamilton, F. H. Wilt, S. Weiner, and L. Addadi, "The transient phase of amorphous calcium carbonate in sea urchin larval spicules: the involvement of proteins and magnesium ions in its formation and stabilization," *Advanced Functional Materials*, vol. 13, no. 6, pp. 480–486, 2003.

[2] E. Beniash, J. Aizenberg, L. Addadi, and S. Weiner, "Amorphous calcium carbonate transforms into calcite during sea urchin larval spicule growth," *Proceedings of the Royal Society of London, Series B: Biological Sciences*, vol. 264, no. 1380, pp. 461–465, 1997.

[3] I. M. Weiss, N. Tuross, L. Addadi, and S. Weiner, "Mollusc larval shell formation: amorphous calcium carbonate is a precursor phase for aragonite," *The Journal of Experimental Zoology*, vol. 293, no. 5, pp. 478–491, 2002.

[4] G. Zhang and J. Xu, "From colloidal nanoparticles to a single crystal: new insights into the formation of nacre's aragonite tablets," *Journal of Structural Biology*, vol. 182, no. 1, pp. 36–43, 2013.

[5] G. Zhang, "Biomineralization on the wavy substrate: shape transition of nacreous tablets from pyramids of amorphous nanoparticles to dome-capped prisms of single crystals," *Acta Biomaterialia*, vol. 36, pp. 277–285, 2016.

[6] Y. Ma and Q. Feng, "A crucial process: organic matrix and magnesium ion control of amorphous calcium carbonate crystallization on β-chitin film," *CrystEngComm*, vol. 17, no. 1, pp. 32–39, 2015.

[7] S. Weiner, W. Traub, and S. B. Parker, "Macromolecules in mollusc shells and their functions in biomineralization," *Philosophical Transactions of the Royal Society B: Biological Sciences*, vol. 304, no. 1121, pp. 425–434, 1984.

[8] Y. Levi-Kalisman, G. Falini, L. Addadi, and S. Weiner, "Structure of the nacreous organic matrix of a bivalve mollusk shell examined in the hydrated state using Cryo-TEM," *Journal of Structural Biology*, vol. 135, no. 1, pp. 8–17, 2001.

[9] F. Song, A. K. Soh, and Y. L. Bai, "Structural and mechanical properties of the organic matrix layers of nacre," *Biomaterials*, vol. 24, no. 20, pp. 3623–3631, 2003.

[10] A. Lin and M. A. Meyers, "Growth and structure in abalone shell," *Materials Science and Engineering: A*, vol. 390, no. 1-2, pp. 27–41, 2005.

[11] L. Addadi, D. Joester, F. Nudelman, and S. Weiner, "Mollusk shell formation: a source of new concepts for understanding biomineralization processes," *Chemistry - A European Journal*, vol. 12, no. 4, pp. 980–987, 2006.

[12] J. H. E. Cartwright and A. G. Checa, "The dynamics of nacre self-assembly," *Journal of The Royal Society Interface*, vol. 4, no. 14, pp. 491–504, 2007.

[13] L. Xie, X. X. Wang, and J. Li, "The SEM and TEM study on the laminated structure of individual aragonitic nacre tablet in freshwater bivalve *H. cumingii* Lea shell," *Journal of Structural Biology*, vol. 169, no. 1, pp. 89–94, 2010.

[14] I. Almagro, P. Drzymała, K. Berent et al., "New crystallographic relationships in biogenic aragonite the crossed-lamellar microstructures of mollusks," *Crystal Growth & Design*, vol. 16, no. 4, pp. 2083–2093, 2016.

[15] G. Falini, S. Fermani, and A. Ripamonti, "Crystallization of calcium carbonate salts into beta-chitin scaffold," *Journal of Inorganic Biochemistry*, vol. 91, no. 3, pp. 475–480, 2002.

[16] N. H. Munro and K. M. McGrath, "Biomimetic approach to forming chitin/aragonite composites," *Chemical Communications*, vol. 48, no. 39, pp. 4716–4718, 2012.

[17] H. Kintsu, T. Okumura, L. Negishi et al., "Crystal defects induced by chitin and chitinolytic enzymes in the prismatic layer of *Pinctada fucata*," *Biochemical and Biophysical Research Communications*, vol. 489, no. 2, pp. 89–95, 2017.

[18] F. H. Shen, Q. L. Feng, and C. M. Wang, "The modulation of collagen on crystal morphology of calcium carbonate," *Journal of Crystal Growth*, vol. 242, no. 1-2, pp. 239–244, 2002.

[19] C. Cheng, Z. Shao, and F. Vollrath, "Silk fibroin-regulated crystallization of calcium carbonate," *Advanced Functional Materials*, vol. 18, no. 15, pp. 2172–2179, 2008.

[20] T. Wang, D. Porter, and Z. Shao, "The intrinsic ability of silk fibroin to direct the formation of diverse aragonite aggregates," *Advanced Functional Materials*, vol. 22, no. 2, pp. 435–441, 2012.

[21] Z. Huang and G. Zhang, "Biomimetic synthesis of aragonite nanorod aggregates with unusual morphologies using a novel template of natural fibrous proteins at ambient condition," *Crystal Growth & Design*, vol. 12, no. 4, pp. 1816–1822, 2012.

[22] Z. Q. Huang and G. S. Zhang, "Influence of acid-soluble proteins from bivalve *Siliqua radiata* ligaments on calcium carbonate crystal growth," *Journal of Crystal Growth*, vol. 448, pp. 64–69, 2016.

[23] O. Grassmann, G. Müller, and P. Löbmann, "Organic-inorganic hybrid structure of calcite crystalline assemblies grown in a gelatin hydrogel matrix relevance to biomineralization," *Chemistry of Materials*, vol. 14, no. 11, pp. 4530–4535, 2002.

[24] O. Grassmann and P. Löbmann, "Biomimetic nucleation and growth of $CaCO_3$ in hydrogels incorporating carboxylate groups," *Biomaterials*, vol. 25, no. 2, pp. 277–282, 2004.

[25] A. Hayashi, T. Nakamura, and T. Watanabe, "Fabrication of a nacre-like aragonite/PAA multilayer film on a nacre substrate," *Crystal Growth & Design*, vol. 10, no. 12, pp. 5085–5091, 2010.

[26] R. Liu, X. Xu, H. Pan, W. Yan, and R. Tang, "Aragonite crystals formation on nacre substrate," *Journal of Crystal Growth*, vol. 351, no. 1, pp. 41–46, 2012.

[27] J. Chen, Y. Huang, M. Su, K. Cheng, and Y. Zhao, "Biomimetic synthesis of oriented aragonite crystals and nacre-like composite material by controlling the fluid type," *Powder Technology*, vol. 302, pp. 455–461, 2016.

[28] E. C. Keene, J. S. Evans, and L. A. Estroff, "Matrix interactions in biomineralization: aragonite nucleation by an intrinsically disordered nacre polypeptide, n16N, associated with a β-chitin substrate," *Crystal Growth & Design*, vol. 10, no. 3, pp. 1383–1389, 2010.

[29] R. A. Metzler, J. S. Evans, C. E. Killian et al., "Nacre protein fragment templates lamellar aragonite growth," *Journal of the American Chemical Society*, vol. 132, no. 18, pp. 6329–6334, 2010.

[30] C. Pan, D. Fang, G. Xu et al., "A novel acidic matrix protein, PfN44, stabilizes magnesium calcite to inhibit the crystallization of aragonite," *The Journal of Biological Chemistry*, vol. 289, no. 5, pp. 2776–2787, 2014.

[31] Y. P. Du, H. H. Chang, S. Y. Yang et al., "Study of binding interaction between Pif80 protein fragment and aragonite," *Scientific Reports*, vol. 6, no. 1, pp. 1–10, 2016.

[32] Z. Huang and G. Zhang, "Identification and secondary structure analysis of a keratin-like fibrous protein discovered in ligament of the bivalve *Siliqua radiata*," *Biochemistry*, vol. 76, no. 11, pp. 1227–1232, 2011.

[33] L. Qiao, Q. Feng, and S. Lu, "In vitro growth of nacre-like tablet forming: from amorphous calcium carbonate, nanostacks to hexagonal tablets," *Crystal Growth & Design*, vol. 8, no. 5, pp. 1509–1514, 2008.

[34] S. Hunt, "Chemical and physical studies of the chitinous siphon sheath in the lamellibranch *Lutraria lutraria* L. and its relationship to the periostracum," *Comparative Biochemistry and Physiology*, vol. 45, no. 2, pp. 311–323, 1973.

[35] S. Weiner and W. Traub, "X-ray diffraction study of the insoluble organic matrix of mollusk shells," *FEBS Letters*, vol. 111, no. 2, pp. 311–316, 1980.

[36] G. Falini, S. Weiner, and L. Addadi, "Chitin-silk fibroin interactions relevance to calcium carbonate formation in invertebrates," *Calcified Tissue International*, vol. 72, no. 5, pp. 548–554, 2003.

[37] J. Brugnerotto, J. Lizardi, F. M. Goycoolea, W. Argüelles-Monal, J. Desbrières, and M. Rinaudo, "An infrared investigation in relation with chitin and chitosan characterization," *Polymer*, vol. 42, no. 8, pp. 3569–3580, 2001.

[38] H. Rasti, K. Parivar, J. Baharara, M. Iranshahi, and F. Namvar, "Chitin from the mollusc chiton: extraction, characterization and chitosan preparation," *Iranian Journal of Pharmaceutical Research*, vol. 16, no. 1, pp. 366–379, 2017.

[39] K. M. Rudall, "Chitin and its association with other molecules," *Journal of Polymer Science Part C*, vol. 28, no. 1, pp. 83–102, 1969.

[40] E. S. Abdou, K. S. A. Nagy, and M. Z. Elsabee, "Extraction and characterization of chitin and chitosan from local sources," *Bioresource Technology*, vol. 99, no. 5, pp. 1359–1367, 2008.

[41] A. Phuruangrata, T. Thongtemb, and S. Thongtem, "Characterization of starfruit-like $PbWO_4$ microstructured clusters synthesized by a solution route," *Journal of Ceramic Processing Research*, vol. 13, pp. 514–516, 2012.

[42] L. Vigderman and E. R. Zubarev, "Starfruit-shaped gold nanorods and nanowires: synthesis and SERS characterization," *Langmuir*, vol. 28, no. 24, pp. 9034–9040, 2012.

[43] J. Shao, X. Li, Q. Qu, and H. Zheng, "One-step hydrothermal synthesis of hexangular starfruit-like vanadium oxide for high power aqueous supercapacitors," *Journal of Power Sources*, vol. 219, pp. 253–257, 2012.

[44] R. L. Penn and J. F. Banfield, "Morphology development and crystal growth in nanocrystalline aggregates under hydrothermal conditions: insights from titania," *Geochimica et Cosmochimica Acta*, vol. 63, no. 10, pp. 1549–1557, 1999.

[45] T. Yui, N. Taki, J. Sugiyama, and S. Hayashi, "Exhaustive crystal structure search and crystal modeling of β-chitin," *International Journal of Biological Macromolecules*, vol. 40, no. 4, pp. 336–344, 2007.

[46] X. Zou, B. Liu, Q. Li et al., "One-step synthesis, growth mechanism and photoluminescence properties of hollow GeO_2 walnuts," *CrystEngComm*, vol. 13, no. 3, pp. 979–984, 2011.

[47] G. Mettela, R. Boya, D. Singh, G. V. P. Kumar, and G. U. Kulkarni, "Highly tapered pentagonal bipyramidal Au microcrystals with high index faceted corrugation: synthesis and optical properties," *Scientific Reports*, vol. 3, no. 1, p. 1793, 2013.